

Depth-Dependent Organization and Dynamics of Archaeal and Eukaryotic Membranes: Development of Membrane Anisotropy Gradient with Natural Evolution

Hirak Chakraborty,^{*,†,‡} Sourav Haldar,^{†,⊥} Parkson Lee-Gau Chong,[§] Mamata Kombrabail,^{||} G. Krishnamoorthy,^{||,#} and Amitabha Chattopadhyay^{*,†}

[†]CSIR-Centre for Cellular and Molecular Biology, Uppal Road, Hyderabad 500 007, India

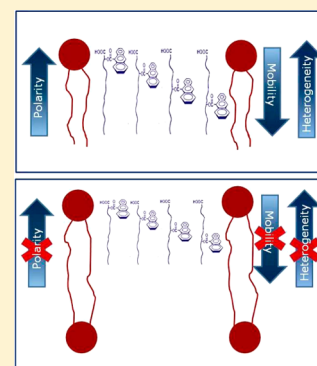
[‡]School of Chemistry, Sambalpur University, Burla, Odisha 768 019, India

[§]Department of Medical Genetics & Molecular Biochemistry, Temple University School of Medicine, Philadelphia, Pennsylvania 19140, United States

^{||}Department of Chemical Sciences, Tata Institute of Fundamental Research, Homi Bhabha Road, Mumbai 400 005, India

S Supporting Information

ABSTRACT: The lipid composition of archaea is unique and has been correlated with increased stability under extreme environmental conditions. In this article, we have focused on the evolution of membrane organization and dynamics with natural evolution. Dynamic anisotropy along the membrane normal (i.e., gradients of mobility, polarity, and heterogeneity) is a hallmark of fluid phase diester or diether phospholipid membranes. We monitored gradients of mobility, polarity, and heterogeneity along the membrane normal in membranes made of a representative archaeal lipid using a series of membrane depth-dependent fluorescent probes, and compared them to membranes prepared from a typical diether lipid from higher organisms (eukaryotes). Our results show that the representative dynamic anisotropy gradient along the membrane normal is absent in membranes made from archaeal lipids. We hypothesize that the dynamic gradient observed in membranes of diester and diether phospholipids is a consequence of natural evolution of membrane lipids in response to the requirement of carrying out complex cellular functions by membrane proteins.



INTRODUCTION

Biological membranes act as a selective permeable barrier that provides cellular identity and compartmentalization. Morphological compartmentalization has long been recognized as a physical prerequisite for Darwinian evolution.^{1,2} Apart from its role in morphological compartmentalization, membranes also represent the meeting point of lipids and proteins.³ Dynamic anisotropy along the bilayer normal is a hallmark of biological membranes.^{4–7} The interfacial region of the membrane is ordered and anisotropic due to intermolecular hydrogen bonding and restricted water molecules, whereas the center of the bilayer is almost isotropic and fluid in nature. This results in a gradient of polarity, order (fluidity), segmental motion, and water penetration along the *z*-axis of the membrane. Interestingly, we have recently shown that in addition to the inherent lateral heterogeneity,^{8–10} membranes also maintain an intrinsic heterogeneity along the bilayer normal.¹¹ Taken together, the biological membrane provides a unique asymmetric environment for transmembrane domains of proteins. In addition, the distribution of amino acids along the bilayer normal in a transmembrane domain of a membrane-spanning protein appears to be highly asymmetric to maintain the structural as well as functional integrity.^{12,13} This could

indicate the parallel evolution of lipids and membrane spanning regions of proteins across natural evolution.¹⁴

The chemical nature of the amphipathic lipid molecules has evolved considerably from primitive to contemporary organisms.^{1,14,15} The genesis of this evolution could be to satisfy the need of an accommodative meeting point of lipids and proteins from a functional point of view, and to constitute the site of many important cellular functions. The function of biological membranes exhibits tremendous increase with growing complexity of organisms. Contemporary biological membranes have evolved to provide numerous roles including compartmentalization, energy transduction, nutrient and ion transport, signal transduction, and enzyme-catalyzed metabolic reactions. While cells have evolved to use diester or diether (or a mixture such as in plasmalogens) glycerophospholipids for their membranes, the membrane lipid composition of cells across natural evolution is very different.^{1,15}

Archaea constitute a domain of single cell microorganisms and are classified as a separate domain in a three-domain system. Their ability to thrive in conditions that would

Received: July 27, 2015

Revised: September 14, 2015

Published: October 7, 2015

otherwise be lethal (such as high temperature and low pH) has led to the interest in studying the properties of their membranes.¹⁶ The membrane lipid composition of archaea is unique¹⁷ and is responsible for their survival in extreme environments.^{18,19} The major component of the plasma membrane in thermoacidophilic archaea is bipolar tetraether lipids. For example, in the thermoacidophilic archaea *Sulfolobus acidocaldarius*, ~90% of the total lipids are bipolar tetraether lipids.^{20,21} Among bipolar tetraether lipids, the polar lipid fraction E (PLFE) is one of the major constituents.²² PLFE contains a mixture of tetraether lipids with either a glycerol dialkyl nonitol tetraether (GDNT) or a glycerol dialkyl glycerol tetraether (GDGT) skeleton (see Figure S1). Both GDNT and GDGT consist of a pair of 40-carbon phytanyl hydrocarbon chains, and each of the biphytanyl chains contains up to four cyclopentane rings depending on its growth temperature.²³ The unique structure of archaeal lipids is believed to be a contributing factor in the thermal stability of archaeal membranes of the thermoacidophilic type.

In this article, we have elucidated the evolution of membrane organization and dynamics with natural evolution. For this, we explored the dynamic anisotropy gradient along the membrane normal of PLFE (archaeal lipid) membranes and compared the results to membranes prepared from ether lipids of higher organisms (eukaryotes). We have chosen 1,2-dihexadecyl-*sn*-glycero-3-phosphocholine (DHPC) as a representative higher organism lipid because it contains an ether linkage similar to PLFE (Figure S1). We monitored the dynamic gradient along the membrane normal by utilizing a series of depth-dependent fluorescent probes inserted in PLFE and DHPC membranes. Our results show that the pronounced dynamic gradient characteristic of eukaryotic membranes is lacking in archaeal lipid membranes. These results constitute one of the early reports comparing depth-dependent membrane order, polarity, heterogeneity, and dynamics between archaeal and eukaryotic membranes, and demonstrate the evolution of dynamic anisotropy along the membrane normal with natural evolution.

EXPERIMENTAL SECTION

Materials. PLFE lipids were extracted from *Sulfolobus acidocaldarius*, grown aerobically and heterotrophically at 80 °C and at pH 2.5, as previously described.^{22,24} DHPC was purchased from Avanti Polar lipids (Alabaster, AL). 1,2-Dimyristoyl-*sn*-glycero-3-phosphocholine (DMPC) was obtained from Sigma Chemical Co. (St. Louis, MO). *n*-AS probes (2-, 6-, 9-, and 12-(9-anthroyloxy)stearic acid) were purchased from Molecular Probes (Eugene, OR). Concentrations of stock solutions of *n*-AS probes in methanol were estimated using the molar extinction coefficient (ϵ) of 8000 M⁻¹ cm⁻¹ at 361 nm.¹¹ Purity of DHPC was checked by thin layer chromatography on precoated silica gel plates from Merck (Darmstadt, Germany) in chloroform/methanol/water (65:35:5, v/v/v), and was found to give one spot with a phosphate-sensitive spray and subsequent charring.²⁵ The concentration of DHPC was determined by phosphate assay after total digestion by perchloric acid.²⁶ DMPC was used as an internal standard to assess the completeness of lipid digestion. Solvents used were of spectroscopic grade, and water was purified through a Millipore (Bedford, MA) Milli-Q system and used throughout.

Preparation of Vesicles. All experiments involving DHPC were carried out using large unilamellar vesicles (LUVs) containing 1 mol % of *n*-AS (2-, 6-, 9-, or 12-AS) probe, as described previously.¹¹ LUVs of PLFE containing 2 mol % *n*-AS probe were used. For this, 320 nmol of PLFE in chloroform/ethanol (9:1, v/v) was mixed with 6.4 nmol of the probe in ethanol. Details of vesicle preparation are provided in the

Supporting Information. All experiments were carried out at ~67 °C for both PLFE and DHPC membranes at pH 5.

Steady State Fluorescence Measurements. Steady state fluorescence measurements were performed with a Fluorolog-3 model FL3-22 spectrofluorometer (Horiba Jobin Yvon, Edison, NJ) using 1 cm path length quartz cuvettes. Details of steady-state fluorescence measurements are provided in the Supporting Information.

Time-Resolved Fluorescence Measurements and Maximum Entropy Method (MEM) Analysis. Time-resolved fluorescence intensity decay measurements were carried out using a time-correlated single photon counting (TCSPC) setup as described elsewhere.¹¹ More details are provided in the Supporting Information.

Time-Resolved Fluorescence Anisotropy. Time-resolved fluorescence anisotropy was analyzed as described previously.^{9,27,28} Details of these measurements are described in the Supporting Information.

Calculation of Wobbling-in-Cone Angle. The fluorescent probe (*n*-AS) is covalently attached to stearic acid and embedded in the membrane. The extent of probe wobbling within the membrane depends on the order (fluidity) of the membrane. The wobbling motion can be modeled as wobbling within a cone, whose semi angle (θ) can be calculated using the Kinosita model.²⁹ Details on calculation of wobbling-in-cone angle are provided in the Supporting Information.

RESULTS

In order to explore the dynamic gradient along the membrane normal and its modulation across natural evolution, we explored the order (fluidity), polarity, and heterogeneity of PLFE and DHPC membranes using a series of depth-dependent fluorescent probes. To explore membrane properties at varying depths along the *z*-axis, we utilized anthroyloxy stearic acids (AS), in which an anthracene group is attached by an ester linkage to various carbon atoms (denoted as *n*) of the alkyl chain. It has been previously demonstrated that the anthroyloxy probes used in this work are localized progressively with increasing depths as the site of attachment of the anthroyloxy group is moved from 2- to 12-position.³⁰

Depth-Dependent Membrane Order and Polarity. Diester or diether glycerophospholipid membranes typically exhibit a considerable degree of order (fluidity) and polarity gradient along the membrane normal.^{4–7} While the center of the bilayer is extremely fluid and hydrophobic, the upper portion, only a few angstroms away toward the membrane surface, is highly ordered and hydrophilic. As a direct consequence of such an anisotropic transmembrane disposition, membranes offer a unique environment to membrane-spanning proteins and peptides, thereby influencing their structure and function. The transmembrane domain of a protein has distinct stretches of hydrophobic amino acids, and the distribution of amino acids is highly asymmetric along the axis perpendicular to the membrane plane.³¹ The physicochemical properties of the membrane interface vary depending on the type of linkage and type of headgroup,³² whereas the properties of the hydrophobic core are guided by the nature of the fatty acyl tails. The archaeal membranes are extraordinarily stable. This is attributed to the chemical nature of the hydrophilic head and the hydrophobic tail of the bipolar tetraether lipids. The presence of branched methyl groups, tetraether linkage, and cyclopentane rings contribute to a highly ordered core of archaeal membranes, and an extensive network of hydrogen bonds between the sugar or phosphate residues provides a highly ordered interface (see Figure S1).^{33,34}

An interesting feature of *n*-AS probes that makes them environment-sensitive is the relatively large change in dipole

moment upon excitation.³⁵ This results in a large Stokes' shift³⁶ and makes *n*-AS probes sensitive to the immediate environment. Steady state fluorescence anisotropy and fluorescence lifetime serve as sensitive indicators of membrane order and polarity. Figure 1A shows fluorescence anisotropy of *n*-AS

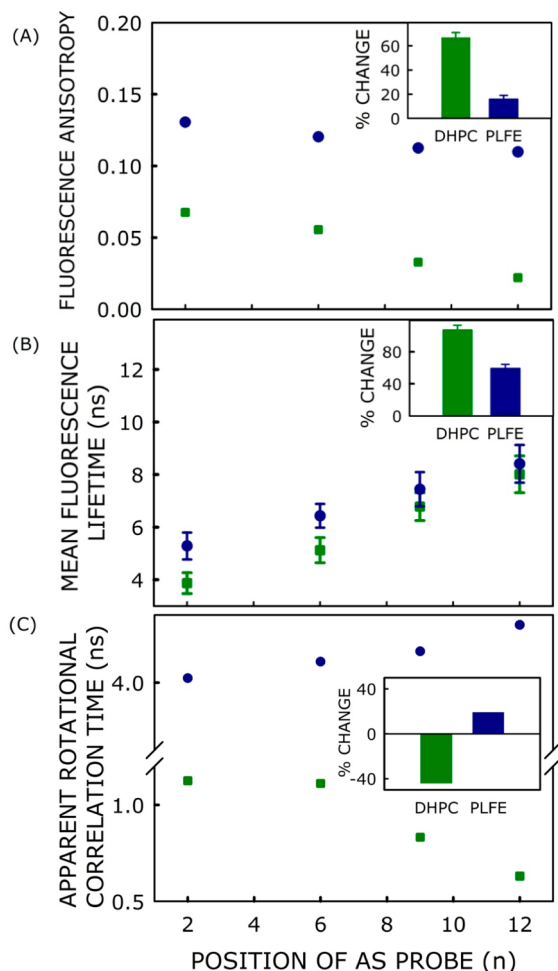


Figure 1. Membrane order and polarity gradients are steeper in DHPC membranes relative to PLFE membranes. Change in (A) steady state fluorescence anisotropy, (B) mean fluorescence lifetime, and (C) apparent rotational correlation time of 2-AS, 6-AS, 9-AS, and 12-AS in LUVs of DHPC (green ■) and PLFE (blue ●). The ratio of probe to lipid was 1/100 (mol/mol) for DHPC and 1/50 (mol/mol) for PLFE, and the concentration of DHPC was 0.43 mM and that of PLFE was 0.21 mM. Experiments were carried out at $\sim 67^\circ\text{C}$ for both PLFE and DHPC membranes at pH 5. The excitation wavelength was 360 nm for anisotropy measurements and 366 nm for lifetime measurements for both lipids. Insets show the percent changes in fluorescence anisotropy, mean fluorescence lifetime, and apparent rotational correlation time between 2-AS and 12-AS. See the Experimental Section for other details.

probes in DHPC and PLFE membranes. The figure shows that the anisotropy of *n*-AS probes drops sharply along the bilayer normal in DHPC membranes. We interpret the depth-dependent reduction in fluorescence anisotropy with the concomitant reduction in membrane order along the membrane normal (it should be noted that information on fluorescence lifetime is required for correct interpretation of fluorescence anisotropy data; see below). In contrast, the corresponding change in fluorescence anisotropy is rather

modest in the case of PLFE membranes. This indicates that the sharp gradient of membrane order, characteristic of eukaryotic membranes, is lacking in PLFE membranes. Nonetheless, all four *n*-AS probes report much higher fluorescence anisotropy values in PLFE membranes as compared to their counterparts in DHPC membranes. This indicates that PLFE membranes are more ordered (less fluid) at all depths along the membrane normal as compared to DHPC membranes. The percentage loss of anisotropy between the shallow (2-AS) and deep (12-AS) probes is shown in the inset of Figure 1A. As is evident, the change in fluorescence anisotropy is considerably higher ($\sim 68\%$) in DHPC membranes relative to the modest change ($\sim 16\%$) in PLFE membranes. This clearly indicates that the gradient of fluidity (order) in DHPC membranes is more pronounced relative to PLFE membranes.

Intensity-averaged fluorescence lifetimes of *n*-AS probes in PLFE and DHPC membranes are plotted in Figure 1B. As is apparent from the figure, the lifetime of a given *n*-AS probe in PLFE membranes is in general higher than the corresponding lifetime in DHPC membranes. This suggests that the environment of *n*-AS probes is less polar in nature in PLFE membranes relative to DHPC membranes. This could be due to overall tighter membrane packing (from both H-bonding and membrane rigidity/compactness) in PLFE membranes, thereby reducing water penetration.³⁷ The percentage change in fluorescence lifetime between 2-AS and 12-AS is much higher for DHPC membranes ($\sim 107\%$) than for PLFE membranes ($\sim 59\%$). This means that the polarity gradient is steeper in DHPC membranes, similar to the steeper gradient in membrane order. In addition, the position of the fluorescence emission maximum also supports that the *n*-AS probes experience more hydrophobic environment in PLFE membranes. The emission maximum of a given *n*-AS probe in PLFE membranes in general exhibits blue shift relative to the emission maximum in DHPC membranes (Figure S2).

Because anisotropy changes are known to be influenced by changes in fluorescence lifetime, we calculated the apparent (average) rotational correlation times for *n*-AS probes in DHPC and PLFE membranes using Perrin's equation:³⁸

$$\tau_c = \frac{\langle \tau \rangle r}{r_0 - r} \quad (1)$$

where r_0 is the limiting (fundamental) anisotropy of the anthroyloxy group, r is the steady state anisotropy (Figure 1A), and $\langle \tau \rangle$ is the mean fluorescence lifetime from Figure 1B. Although Perrin's equation is not strictly applicable to this system, it is assumed that this equation will apply to a first approximation, especially because we used mean fluorescence lifetimes for the analysis of multiple component lifetimes. The values of the apparent rotational correlation times, calculated using eq 1 with a r_0 value of 0.3,³⁹ are shown in Figure 1C. The percentage change of rotational correlation time between the shallow (2-AS) and deep (12-AS) probes is shown in the inset of Figure 1C. As is apparent from Figure 1C, the trend in change in rotational correlation time is opposite in the case of DHPC and PLFE membranes. For example, while the rotational correlation time displays a considerable decrease ($\sim 44\%$) in DHPC membranes, it exhibits a modest increase ($\sim 19\%$) in PLFE membranes. These results clearly demonstrate that while DHPC has a distinct mobility gradient along the membrane normal, such a gradient is absent in PLFE membranes (see later, Figure 5).

Depth-Dependent Wobbling-in-Cone Angle. The most popular model of dynamics of a covalently attached fluorophore molecule in the membrane is the wobbling-in-cone model.²⁹ The wobbling of a fluorophore in the membrane depends on membrane order and steric crowding. Higher cone angle indicates unhindered (free) rotation of the probe in the membrane due to fluid (less ordered) nature of the membrane. The cone angles of *n*-AS probes, calculated from the time-resolved anisotropy decay (see [Experimental Section](#)), in DHPC and PLFE membranes are shown in [Figure 2](#). The

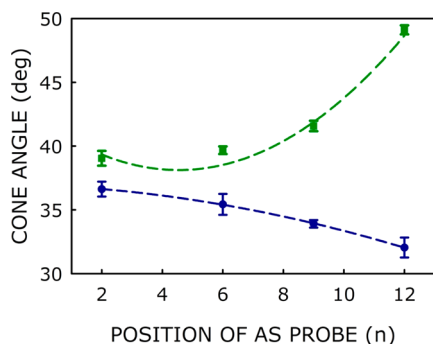


Figure 2. Position-dependent differential wobbling-in-cone angle of *n*-AS probes in DHPC and PLFE membranes. Variation of cone angle of *n*-AS probes ($n = 2, 6, 9,$ and 12) in LUVs of DHPC (green ■) and PLFE (blue ●) with deeper localization of the fluorophore moiety in the membrane interior. The cone angle was calculated from time-resolved fluorescence anisotropy decay measurements (see the [Experimental Section](#) for details). Lines joining the data points are provided merely as viewing guides. Other conditions are the same as in [Figure 1](#).

cone angle in DHPC membranes changes from 39° to 49° between 2-AS and 12-AS, that is, exhibits progressive increase ($\sim 26\%$) with the point of attachment of the anthroyloxy probe (depth) and is consistent with the reduction in membrane order with depth ([Figure 1A](#)). The values of cone angle for *n*-AS probes in DHPC membranes are comparable with that in dimyristoylphosphatidylcholine membranes for the styrylpyridinium probe RH421.⁴⁰ The change in cone angle of *n*-AS probes in PLFE membranes shows an interesting trend. The cone angle is reduced ($\sim 12\%$) along the membrane normal, although the extent of change is less. This means the angle of probe wobbling becomes narrower along the membrane normal. The decrease in cone angle might be explained considering the presence of branched methyl groups and cyclopentane rings in PLFE. These branched methyl groups and cyclopentane rings ([Figure S1](#)) in PLFE membranes make the hydrophobic region sterically crowded, and change the membrane order, thereby hindering probe rotation. The corresponding rotational correlation times (φ_i) from the analysis of the fitted anisotropy decays are shown in [Table S1](#). It is interesting to note that the fraction (β_1) corresponding to slow rotating component (φ_1) exhibits an increase in PLFE membranes, and shows reduction in DHPC membranes along the membrane normal.

Depth-Dependent Solvent Relaxation. Properties such as polarity, fluidity, segmental motion, ability to form hydrogen bonds, and extent of water penetration vary in a depth-dependent manner in the membrane. As a result of such anisotropy along the membrane normal, a gradient of mobility of solvent molecules at different depths of the membrane is

induced. We utilized red edge excitation shift (REES) to monitor water penetration and dynamics at different depths in DHPC and PLFE membranes. REES relies on slow solvent reorientation in the excited state of a fluorophore, with each excitation wavelength selectively exciting a different population of fluorophores.^{6,7,31} [Figure 3](#) shows the magnitude of REES for

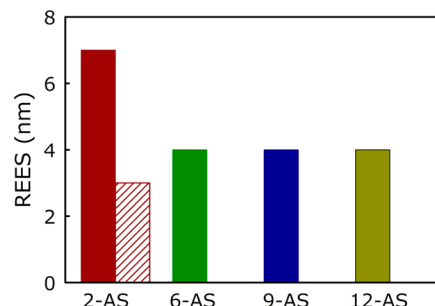


Figure 3. Differential REES exhibited by *n*-AS probes in DHPC and PLFE membranes. REES of *n*-AS probes in PLFE (solid bar) and DHPC (hatched bar) membranes for 2-AS, 6-AS, 9-AS, and 12-AS. The excitation wavelength was varied from 360 to 410 nm (for details of emission wavelength change, see [Figure S3](#)). All other conditions are as in [Figure 1](#). The spectral shifts obtained with different sets of samples were identical in most cases. In other cases, the values were within ± 1 nm of those reported. See the [Experimental Section](#) for other details.

n-AS probes in DHPC and PLFE membranes. The emission maximum of 2-AS in DHPC membranes displays 3 nm shift (from 470 to 473 nm) when the excitation wavelength was changed from 360 to 410 nm (see [Figure S3](#)). Such type of shift in the wavelength of emission maximum caused by a change in the excitation wavelength is representative of REES. REES of 3 nm indicates that the anthroyloxy moiety in 2-AS is localized in a motionally restricted region of the DHPC membrane that offers considerable resistance to solvent reorientation in the excited state. Deeper *n*-AS probes (6-, 9-, and 12-AS) do not show any excitation wavelength dependent shift in emission maximum, which implies that the motional restriction is completely absent in the location of deeper *n*-AS probes (or lack of polar solvent in the deeper regions of the membrane), in agreement with our previous results.⁴¹ This indicates differential extents of motional restriction along the bilayer normal in DHPC membranes. Interestingly, 2-AS in PLFE membranes shows REES of 7 nm (from 462 to 469 nm) for the same excitation wavelength range ([Figures 3](#) and [S3](#)). The deeper probes (6-AS, 9-AS, and 12-AS) show REES of 4 nm in PLFE membranes. This shows that the environment of 2-AS is more restricted in PLFE membranes (relative to DHPC membranes) and the motional restriction persists even in deeper locations along the membrane normal, in agreement with fluorescence anisotropy measurements. This could be due to the presence of branched methyl groups and cyclopentane rings in the hydrophobic region in PLFE membranes ([Figure S1](#)).

Depth-Dependent Membrane Heterogeneity. Fluorescence decay kinetics of probes incorporated in complex organized assemblies typically exhibits considerable level of heterogeneity. The lifetime distribution offers a powerful method for characterizing such heterogeneity in complex systems such as membranes.^{42,43} MEM is a model-free and robust methodology for analyzing fluorescence lifetime distribution. The full width at half maximum (FWHM) of the

lifetime distribution is correlated with the degree of heterogeneity sensed by the fluorophore.^{9,11} We have previously shown that the environmental heterogeneity of *n*-AS probes varies considerably depending on its location along the membrane normal.¹¹ The shallow probe 2-AS at the membrane interface experiences maximum heterogeneity, while the heterogeneity experienced by the deep probe 12-AS is less.¹¹ This results in a wider FWHM for 2-AS as compared to 12-AS. We analyzed the fluorescence lifetime decay profiles of *n*-AS probes using MEM in DHPC and PLFE membranes, and the FWHM values extracted from these data are shown in Figure 4 (the lifetime distribution profiles are shown in Figure

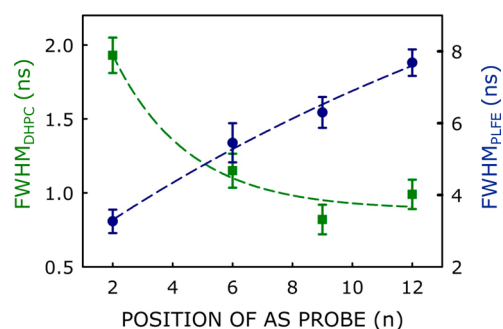


Figure 4. Contrasting membrane heterogeneity profiles in DHPC and PLFE membranes: heterogeneity reduces with depth in DHPC membranes but increases in PLFE membranes. Variation of the width of the fluorescence lifetime distribution (represented as FWHM) of *n*-AS probes in PLFE (blue ●) and DHPC (green ■) membranes. All other conditions are as in Figure 1. Lines joining the data points are provided merely as viewing guides. See the Experimental Section for other details.

S4). In DHPC membranes, FWHM shows reduction with membrane depth (as the probe location becomes deeper), as reported earlier for fluid membranes of diester phospholipids.¹¹ In PLFE membranes, however, FWHM shows an increase with membrane depth. The increase in FWHM in case of PLFE membranes could be attributed to the presence of branched methyl groups and cyclopentane rings in the hydrophobic region in PLFE membranes, which would reduce sampling and increase heterogeneity.

DISCUSSION

In an earlier study, lipid chain dynamics and polarity gradient in membranes of bipolar tetraether lipids was studied by Bartucci et al. and compared to ester lipids.⁴⁴ The dynamic properties of bolalipid membranes have recently been explored by coarse-grain molecular dynamics simulation.⁴⁵ Instead of considering the structure of either GDGT or GDNT, these authors covalently linked two dipalmitoylphosphatidylcholine (DPPC) at two tails, which tends to mimic the bipolar tetraether lipids. The results showed that the variation in order parameter along the membrane normal is rather modest for membranes made of bolalipids, in overall agreement with our results.

About 50% of all genetically encoded proteins in the eukaryotic genome are membrane associated proteins, and it is likely that ~50% of all reactions occurring in a cell take place on membranes.⁴⁶ Membrane proteins constitute ~50% of current targets in all clinical areas.⁴⁷ Because a majority of all membrane proteins are targeted to the plasma membrane, a significant fraction of cellular reactions occur on or close to the plasma membrane. The plasma membrane therefore not only

acts as a selective barrier for the cell, but also serves as a platform for the initiation and regulation of signaling pathways. As stated above, the lipid composition of archaea is unique and has been correlated with increased stability under extreme conditions. In this article, we show that the gradient of dynamics along the bilayer normal, a hallmark of fluid membranes made of diester or diether phospholipids, is absent (or damped) in membranes made of archaeal lipids such as PLFE (see Figure 5 for a schematic representation). These

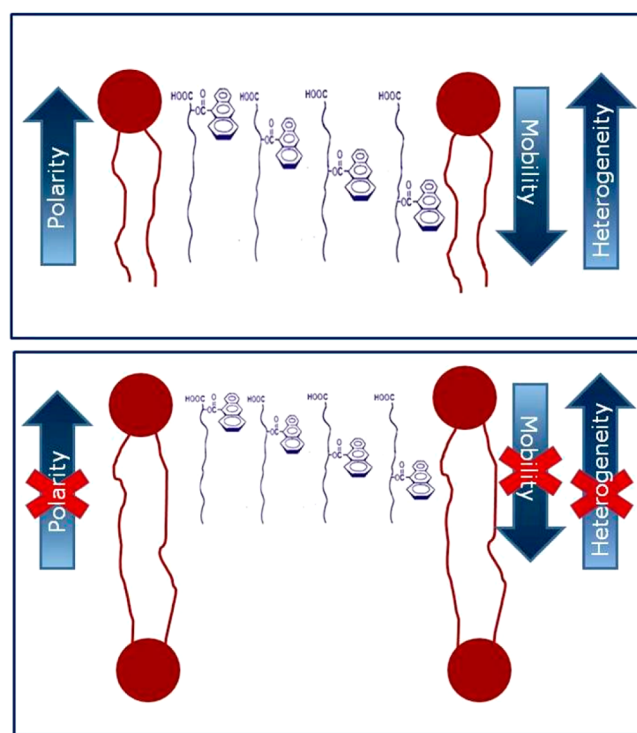


Figure 5. A schematic representation showing the localizations of the anthroxyloxy group in *n*-AS probes in DHPC (top) and PLFE (bottom) membranes. The arrows along the membrane perpendicular (*z*-axis) indicate gradients in polarity, mobility, and heterogeneity along the membrane normal. Gradients of polarity, mobility, and heterogeneity are steeper in DHPC membranes relative to what was observed in PLFE membranes. See text for more details.

results are based on observed changes in membrane order, polarity, packing, motional restriction, and heterogeneity along the membrane for DHPC and PLFE membranes monitored using a variety of steady state and time-resolved fluorescence approaches. We hypothesize here that the dynamic gradient observed in diester and diether phospholipid membranes is a consequence of natural evolution of amphipathic lipid molecules. This is in response to the requirement to fulfill the increasingly stringent criterion of maintaining the higher order function of a wide variety of membrane proteins, essential for cellular viability and increased signaling carried out by membrane proteins in complex eukaryotic cells. In other words, the membrane should provide an optimal environment, in terms of organization and dynamics, for efficient functioning of membrane proteins such as receptors and ion channels. The natural evolution of membrane lipids from archaeal lipids to contemporary eukaryotic lipids is in response to provide an optimal dynamic environment for eukaryotic membrane proteins with their characteristic transmembrane sequence. We therefore envision that a robust bioinformatic analysis of

transmembrane sequences found in archaea and eukaryotes could provide insight into the evolution of membrane proteins.

■ ASSOCIATED CONTENT

Supporting Information

The Supporting Information is available free of charge on the ACS Publications website at DOI: 10.1021/acs.langmuir.5b02760.

Experimental section; Table S1; Figures S1–S4; references (PDF)

■ AUTHOR INFORMATION

Corresponding Authors

*Phone: +91-40-2719-2578. Fax: +91-40-2716-0311. E-mail: amit@ccmb.res.in.

*Phone: +91-8008716419. Fax: +91-663-2430158. E-mail: hirak@suniv.ac.in.

Present Addresses

[†]Section on Integrative Biophysics, Eunice Kennedy Shriver National Institute of Child Health and Human Development, National Institutes of Health, Bethesda, Maryland 20892, United States.

[#]Department of Biotechnology, Anna University, Chennai 600 025, India.

Notes

The authors declare no competing financial interest.

■ ACKNOWLEDGMENTS

Work in A.C.'s laboratory was supported by the Council of Scientific and Industrial Research, Government of India. P.L.-G.C. acknowledges support from NSF DMR-1105277 and CBET-11350841. A.C. and G.K. gratefully acknowledge support from J. C. Bose Fellowship (Department of Science and Technology, Government of India). H.C. thanks the Council of Scientific and Industrial Research (Government of India) for the award of Senior Research Associateship and the University Grants Commission for UGC-Assistant Professor position. S.H. thanks the Council of Scientific and Industrial Research for the award of a Senior Research Fellowship. A.C. is an Adjunct Professor of Tata Institute of Fundamental Research (Mumbai), RMIT university (Melbourne, Australia), Indian Institute of Technology (Kanpur), and Indian Institute of Science Education and Research (Mohali). We thank Md. Jafurulla for help during preparation of the manuscript, G. Aditya Kumar for help in making figures, and members of the Chattopadhyay laboratory for critically reading the manuscript.

■ REFERENCES

- (1) Deamer, D.; Dworkin, J. P.; Sandford, S. A.; Bernstein, M. P.; Allamandola, L. J. The First Cell Membranes. *Astrobiology* **2002**, *2*, 371–381.
- (2) Budin, I.; Szostak, J. W. Expanding Roles for Diverse Physical Phenomena During the Origin of Life. *Annu. Rev. Biophys.* **2010**, *39*, 245–263.
- (3) Escibá, P. V.; González-Ros, J. M.; Goñi, F. M.; Kinnunen, P. K. J.; Vigh, L.; Sánchez-Magraner, L.; Fernández, A. M.; Busquets, X.; Horváth, I.; Barceló-Coblijn, G. Membranes: A Meeting Point for Lipids, Proteins and Therapies. *J. Cell. Mol. Med.* **2008**, *12*, 829–875.
- (4) Seelig, J. Deuterium Magnetic Resonance: Theory and Application to Lipid Membranes. *Q. Rev. Biophys.* **1977**, *10*, 353–418.
- (5) Stubbs, C. D.; Ho, C.; Slater, S. J. Fluorescence Techniques for Probing Water Penetration into Lipid Bilayers. *J. Fluoresc.* **1995**, *5*, 19–28.

- (6) Haldar, S.; Chaudhuri, A.; Chattopadhyay, A. Organization and Dynamics of Membrane Probes and Proteins Utilizing the Red Edge Excitation Shift. *J. Phys. Chem. B* **2011**, *115*, 5693–5706.

- (7) Chattopadhyay, A. Exploring Membrane Organization and Dynamics by the Wavelength-selective Fluorescence Approach. *Chem. Phys. Lipids* **2003**, *122*, 3–17.

- (8) Mukherjee, S.; Maxfield, F. R. Membrane Domains. *Annu. Rev. Cell Dev. Biol.* **2004**, *20*, 839–866.

- (9) Mukherjee, S.; Kombrabail, M.; Krishnamoorthy, G.; Chattopadhyay, A. Dynamics and Heterogeneity of Bovine Hippocampal Membranes: Role of Cholesterol and Proteins. *Biochim. Biophys. Acta, Biomembr.* **2007**, *1768*, 2130–2144.

- (10) Falck, E.; Patra, M.; Karttunen, M.; Hyvönen, M. T.; Vattulainen, I. Impact of Cholesterol on Voids in Phospholipid Membranes. *J. Chem. Phys.* **2004**, *121*, 12676–12689.

- (11) Haldar, S.; Kombrabail, M.; Krishnamoorthy, G.; Chattopadhyay, A. Depth-dependent Heterogeneity in Membranes by Fluorescence Lifetime Distribution Analysis. *J. Phys. Chem. Lett.* **2012**, *3*, 2676–2681.

- (12) Sharpe, H. J.; Stevens, T. J.; Munro, S. A Comprehensive Comparison of Transmembrane Domains Reveals Organelle-specific Properties. *Cell* **2010**, *142*, 158–169.

- (13) Andersen, O. S. Perspectives on Membrane Protein Insertion, Protein-bilayer Interactions, and Amino Acid Side Hydrophobicity. *J. Gen. Physiol.* **2007**, *129*, 351–352.

- (14) Mulikidjanian, A. Y.; Galperin, M. Y.; Koonin, E. V. Co-evolution of Primordial Membranes and Membrane Proteins. *Trends Biochem. Sci.* **2009**, *34*, 206–215.

- (15) Deamer, D. W.; Pashley, R. M. Amphiphilic Components of the Murchison Carbonaceous Chondrite: Surface Properties and Membrane Formation. *Orig. Life Evol. Biosph.* **1989**, *19*, 21–38.

- (16) Oger, P. M.; Cario, A. Adaptation of the Membrane in Archaea. *Biophys. Chem.* **2013**, *183*, 42–56.

- (17) DeLong, E. F. Archaeal Mysteries of the Deep Revealed. *Proc. Natl. Acad. Sci. U.S.A.* **2006**, *103*, 6417–6418.

- (18) van de Vossenberg, J. L. C. M.; Driessen, A. J. M.; Konings, W. N. The Essence of Being Extremophilic: The Role of the Unique Archaeal Membrane Lipids. *Extremophiles* **1998**, *2*, 163–170.

- (19) Koga, Y.; Morii, H. Biosynthesis of Ether-type Polar Lipids in Archaea and Evolutionary Considerations. *Microbiol. Mol. Biol. Rev.* **2007**, *71*, 97–120.

- (20) Kates, M. Archaeobacterial Lipids: Structure, Biosynthesis and Function. *Biochem. Soc. Symp.* **1992**, *58*, 51–72.

- (21) Chong, P. L.-G. Archaeobacterial Bipolar Tetraether Lipids: Physico-chemical and Membrane Properties. *Chem. Phys. Lipids* **2010**, *163*, 253–265.

- (22) Lo, S.-L.; Chang, E. L. Purification and Characterization of a Liposomal-forming Tetraether Lipid Fraction. *Biochem. Biophys. Res. Commun.* **1990**, *167*, 238–243.

- (23) De Rosa, M.; Gambacorta, A.; Nicolaus, B.; Chappe, B.; Albrecht, P. Isoprenoid Ethers: Backbone of Complex Lipids of the Archaeobacterium *Sulfolobus solfataricus*. *Biochim. Biophys. Acta, Lipids Lipid Metab.* **1983**, *753*, 249–256.

- (24) Lo, S.-L.; Montague, C. E.; Chang, E. L. Purification of Glycerol Dialkyl Nonitol Tetraether from *Sulfolobus acidocaldarius*. *J. Lipid Res.* **1989**, *30*, 944–949.

- (25) Baron, C. B.; Coburn, R. F. Comparison of Two Copper Reagents for Detection of Saturated and Unsaturated Neutral Lipids by Charring Densitometry. *J. Liq. Chromatogr.* **1984**, *7*, 2793–2801.

- (26) McClare, C. W. F. An Accurate and Convenient Organic Phosphorus Assay. *Anal. Biochem.* **1971**, *39*, 527–530.

- (27) Paila, Y. D.; Kombrabail, M.; Krishnamoorthy, G.; Chattopadhyay, A. Oligomerization of the Serotonin_{1A} Receptor in Live Cells: A Time-resolved Fluorescence Anisotropy Approach. *J. Phys. Chem. B* **2011**, *115*, 11439–11447.

- (28) Haldar, S.; Chaudhuri, A.; Gu, H.; Koeppe, R. E., II; Kombrabail, M.; Krishnamoorthy, G.; Chattopadhyay, A. Membrane Organization and Dynamics of "Inner Pair" and "Outer Pair"

Tryptophan Residues in Gramicidin Channels. *J. Phys. Chem. B* **2012**, *116*, 11056–11064.

(29) Kinosita, K., Jr.; Kawato, S.; Ikegami, A. A Theory of Fluorescence Polarization Decay in Membranes. *Biophys. J.* **1977**, *20*, 289–305.

(30) Abrams, F. S.; London, E. Extension of the Parallax Analysis of Membrane Penetration Depth to the Polar Region of Model Membranes: Use of Fluorescence Quenching by a Spin-label Attached to the Phospholipid Polar Headgroup. *Biochemistry* **1993**, *32*, 10826–10831.

(31) Chattopadhyay, A.; Haldar, S. Dynamic Insight into Protein Structure Utilizing Red Edge Excitation Shift. *Acc. Chem. Res.* **2014**, *47*, 12–19.

(32) Mukherjee, S.; Chattopadhyay, A. Influence of Ester and Ether Linkage in Phospholipids on the Environment and Dynamics of the Membrane Interface: A Wavelength-selective Fluorescence Approach. *Langmuir* **2005**, *21*, 287–293.

(33) Kao, Y. L.; Chang, E. L.; Chong, P. L.-G. Unusual Pressure Dependence of the Lateral Motion of Pyrene-labeled Phosphatidylcholine in Bipolar Lipid Vesicles. *Biochem. Biophys. Res. Commun.* **1992**, *188*, 1241–1246.

(34) Khan, T. K.; Chong, P. L.-G. Studies of Archaeobacterial Bipolar Tetraether Liposomes by Perylene Fluorescence. *Biophys. J.* **2000**, *78*, 1390–1399.

(35) Werner, T. C.; Hoffman, R. M. Relation between an Excited State Geometry Change and the Solvent Dependence of 9-Methyl Anthroate Fluorescence. *J. Phys. Chem.* **1973**, *77*, 1611–1615.

(36) Garrison, M. D.; Doh, L. M.; Potts, R. O.; Abraham, W. Fluorescence Spectroscopy of 9-Anthroyloxy Fatty Acids in Solvents. *Chem. Phys. Lipids* **1994**, *70*, 155–162.

(37) Mathai, J. C.; Sprott, G. D.; Zeidel, M. L. Molecular mechanisms of water and solute transport across archaeobacterial lipid membranes. *J. Biol. Chem.* **2001**, *276*, 27266–27271.

(38) Lakowicz, J. R. *Principles of Fluorescence Spectroscopy*, 3rd ed.; Springer: New York, 2006.

(39) Tricerri, M. A.; Garda, H. A.; Brenner, R. R. Lipid Chain Order and Dynamics at Different Bilayer Depths in Liposomes of Several Phosphatidylcholines Studied by Differential Polarized Phase Fluorescence. *Chem. Phys. Lipids* **1994**, *71*, 61–72.

(40) Visser, N. V.; van Hoek, A.; Visser, A. J. W. G.; Frank, J.; Apell, H.-J.; Clarke, R. J. Time-resolved fluorescence investigations of the interaction of the voltage-sensitive probe RH421 with lipid membranes and proteins. *Biochemistry* **1995**, *34*, 11777–11784.

(41) Chattopadhyay, A.; Mukherjee, S. Depth-dependent Solvent Relaxation in Membranes: Wavelength-selective Fluorescence as a Membrane Dipstick. *Langmuir* **1999**, *15*, 2142–2148.

(42) Davenport, L. Fluorescence Probes for Studying Membrane Heterogeneity. *Methods Enzymol.* **1997**, *278*, 487–512.

(43) Williams, B. W.; Stubbs, C. D. Properties Influencing Fluorophore Lifetime Distributions in Lipid Bilayers. *Biochemistry* **1988**, *27*, 7994–7999.

(44) Bartucci, R.; Gambacorta, A.; Gliozzi, A.; Marsh, D.; Sportelli, L. Bipolar Tetraether Lipids: Chain Flexibility and Membrane Polarity Gradients from Spin-label Electron Spin Resonance. *Biochemistry* **2005**, *44*, 15017–15023.

(45) Bulacu, M.; Périole, X.; Marrink, S. J. In Silico Design of Robust Bolalipid Membranes. *Biomacromolecules* **2012**, *13*, 196–205.

(46) Zimmerberg, J. Membrane Biophysics. *Curr. Biol.* **2006**, *16*, R272–R276.

(47) Drews, J. Drug Discovery: A Historical Perspective. *Science* **2000**, *287*, 1960–1964.

Supporting Information

Depth-dependent Organization and Dynamics of Archaeal and Eukaryotic Membranes: Development of Membrane Anisotropy Gradient with Natural Evolution

Hirak Chakraborty,^{†,¶,*} Sourav Haldar,^{†,#} Parkson Lee-Gau Chong,[‡] Mamata Kombrabail,[§]
G. Krishnamoorthy,^{§,§} and Amitabha Chattopadhyay^{†,*}

[†]CSIR-Centre for Cellular and Molecular Biology, Uppal Road, Hyderabad 500 007, India;
[¶]School of Chemistry, Sambalpur University, Burla, Odisha 768 019, India; [‡]Department of
Medical Genetics & Molecular Biochemistry, Temple University School of Medicine,
Philadelphia, Pennsylvania, 19140, USA; [§]Department of Chemical Sciences, Tata Institute of
Fundamental Research, Homi Bhabha Road, Mumbai 400 005, India

Present addresses: [#]Section on Integrative Biophysics, Eunice Kennedy Shriver National Institute
of Child Health and Human Development, National Institutes of Health, Bethesda, MD 20892,
USA; [§]Department of Biotechnology, Anna University, Chennai 600 025, India

*Address correspondence to Amitabha Chattopadhyay: Phone: +91-40-2719-2578, Fax: +91-40-
2716-0311, E-mail: amit@ccmb.res.in; or Hirak Chakraborty: Phone: +91-8008716419; Fax:
+91-663-2430158; E-mail: hirak@suniv.ac.in

EXPERIMENTAL SECTION

Preparation of Vesicles. All experiments with DHPC were carried out using large unilamellar vesicles (LUVs) containing 1 mol% of either of 2-, 6-, 9- or 12-AS, as described previously.¹ Briefly, 640 nmol of lipid in chloroform was mixed with 6.4 nmol of the probe in methanol. A few drops of chloroform were added and mixed well, and the samples were dried under a stream of nitrogen while being warmed gently (35 °C). Experiments involving PLFE were carried out using LUVs containing 2 mol% of a given n-AS probe. For this, 320 nmol of PLFE in chloroform was mixed with 6.4 nmol of the probe in ethanol and the same procedure as described for DHPC vesicles preparation was followed. After further drying under a high vacuum for at least 3 h, 1.5 ml of 10 mM sodium acetate, 150 mM sodium chloride, pH 5 buffer was added, and each sample was vortexed for 3 min to disperse the lipids and hydrated for an hour at ~67 °C. LUVs with a diameter of 100 nm were prepared by the extrusion technique using an Avanti Mini-Extruder (Alabaster, AL) as previously described.² Background samples were prepared the same way except that the probes were omitted.

Steady State Fluorescence Measurements. Steady state fluorescence measurements were performed with a Fluorolog-3 Model FL3-22 spectrofluorometer (Horiba Jobin Yvon, Edison, NJ) using 1 cm path length quartz cuvettes. Excitation and emission slits with a nominal band pass of 3 nm were used for all measurements. Background (fluorophore free) intensities of samples were subtracted from each sample spectrum to cancel out any contribution due to the solvent Raman peak and other scattering artifacts. Fluorescence anisotropy measurements were performed using the same instrument. Anisotropy values were calculated using the following equation:³

$$r = \frac{I_{VV} - G \times I_{VH}}{I_{VV} + 2G \times I_{VH}} \quad (1)$$

where $G = I_{HV}/I_{HH}$, (grating correction or G-factor), I_{VV} and I_{VH} are the measured fluorescence intensities with the excitation polarizer vertically oriented and the emission polarizer vertically and horizontally oriented, respectively. All experiments were done with multiple sets of samples and average values of fluorescence anisotropy are shown in the figures. The spectral shifts obtained with different sets of samples were identical in most cases. In other cases, the values were within 1 nm of the ones reported.

Time-Resolved Fluorescence Measurements and MEM Analysis. Time-resolved fluorescence intensity decay measurements were carried out using a time-correlated single photon counting (TCSPC) setup as described elsewhere.¹ For fluorescence lifetime measurements, 1 ps pulses of 732 nm radiation from the Ti-sapphire femto/pico second laser (Spectra Physics, Mountain View, CA), pumped by an Nd-YLF laser (Millenia X, Spectra Physics), were frequency doubled to 366 nm by using a frequency doubler/tripler (GWU, Spectra physics). Fluorescence decay curves were obtained at the laser repetition rate of 4 MHz by a micro-channel plate photomultiplier (model R2809u, Hamamatsu Corp.) coupled to a TCSPC setup. The instrument response function (IRF) at 366 nm was obtained using a dilute colloidal suspension of dried non-dairy creamer. The full width at half maxima (FWHM) of the IRF was 40 ps and number of channels used was 1024. Fluorescence emission of n-AS probes was measured at 460 nm using a combination of a monochromator and a 400 nm cutoff filter. Fluorescence intensity decay was collected from the sample after the excitation with the emission polarizer oriented at the magic angle (54.7°) with respect to the excitation polarizer. To optimize the signal-to-noise ratio, 20,000 photons were collected in the peak channel. All experiments were performed using excitation and emission slits with a nominal bandpass of 3 nm or less. The data stored in the multichannel analyzer were routinely transferred to an IBM PC for analysis. Fluorescence intensity decay curves so obtained were deconvoluted with the instrument response function and analyzed as a sum of exponential terms:

$$F(t) = \sum_i \alpha_i \exp(-t / \tau_i) \quad (2)$$

where $F(t)$ is the fluorescence intensity at time t and α_i is a pre-exponential factor representing the fractional contribution to the time-resolved decay of the component with a lifetime τ_i such that $\sum_i \alpha_i = 1$. The decay parameters were recovered using a nonlinear least-squares iterative fitting procedure based on the Levenberg-Marquardt algorithm.^{4,5} A fit was considered acceptable when plots of the weighted residuals and the autocorrelation function showed random deviation about zero with a minimum χ^2 value not more than 1.2. Fluorescence decays were analyzed by the discrete exponential analysis as well as the maximum entropy method (MEM). Intensity-averaged lifetimes ($\langle \tau \rangle$) for biexponential decays of fluorescence were calculated from the decay times and pre-exponential factors using the following equation:³

$$\langle \tau \rangle = (\alpha_1 \tau_1^2 + \alpha_2 \tau_2^2) / (\alpha_1 \tau_1 + \alpha_2 \tau_2) \quad (3)$$

In the MEM approach,^{6,7} the fluorescence intensity decay ($I(t)$) is analyzed using the model of continuous distribution of lifetimes:

$$I(t) = \int_0^{\infty} \alpha(\tau) \exp(-t / \tau) d\tau \quad (4)$$

where $\alpha(\tau)$ represents the amplitude corresponding to the lifetime τ in the intensity decay. The limits on the above integration are generally set based on the information regarding the system under study and the detection limit of the instrument. We set the lower and the upper limits of the integration as 10 ps and 10 ns, respectively. For practical reasons, the above equation can be written in terms of a discrete sum of exponentials as:

$$I(t) = \sum_{i=1}^N \alpha_i \exp(-t / \tau_i) \quad (5)$$

where N represents the total number of exponentials. In our analysis, N is taken as 150 exponentials equally spaced in the $\log(\tau)$ space between the lower and upper limits. MEM initially starts with a flat distribution of amplitudes $\alpha(\tau)$, that is, assuming that each lifetime has equal contribution in the beginning and arrives at the amplitude distribution that best describes the observed experimental fluorescence intensity decay. The optimization of the amplitude

distribution $\alpha(\tau)$ is carried out in successive cycles by minimizing the χ^2 value (close to 1 in all cases) and maximizing the entropy (S).⁸ The expression used for S is the Shannon-Jayne's entropy function, expressed as $S = -\sum p_i \log p_i$ where $p_i = \alpha_i / \sum \alpha_i$ (6)

Successive iterations provide a distribution that minimizes the χ^2 and maximize S. If the χ^2 criterion is satisfied by many distributions in a particular iteration, then the distribution with maximum entropy is selected. The analysis is terminated when χ^2 reaches the specified lower limit or when χ^2 and $\alpha(\tau)$ show no change in successive iterations. Importantly, MEM analysis gives a lifetime distribution that is robust and model-independent.^{8,9}

Time-Resolved Fluorescence Anisotropy. Time-resolved fluorescence anisotropy was analyzed as described previously.^{6,10,11} The fluorescence intensity decays were collected with the emission polarizer kept at parallel (I_{\parallel}) and perpendicular (I_{\perp}) orientations with respect to the excitation polarizer. Anisotropy was calculated as:

$$r(t) = \frac{I_{\parallel}(t) - GI_{\perp}(t)}{I_{\parallel}(t) + 2GI_{\perp}(t)} \quad (7)$$

where G is the grating factor (G-factor). The G-factor is defined as the ratio of the transmission efficiency of the grating for vertically polarized light to horizontally polarized light. The G factor of the emission collection optics was determined in a separate experiment using a standard sample (IAEDANS). The time-resolved anisotropy decay was analyzed on the basis of the model:

$$\begin{aligned} I_{\parallel}(t) &= I(t)[1 + 2r(t)]/3 \\ I_{\perp}(t) &= I(t)[1 - r(t)]/3 \end{aligned} \quad (8)$$

where $I_{\parallel}(t)$ and $I_{\perp}(t)$ are the decays of the parallel (\parallel) and perpendicular (\perp) components of emission. The equation for time-resolved fluorescence anisotropy can be expressed as combination of exponential decays:

$$r(t) = r_0 \sum_i \beta_i \exp(-t / \phi_i) \quad (9)$$

where ϕ_i and β_i represent the i^{th} rotational correlation time and the corresponding pre-exponential factor in the exponential anisotropy decay such that $\sum \beta_i = 1$. r_0 represents the anisotropy at zero time (initial anisotropy). The goodness of the fit of a given set of observed data and the chosen function was evaluated by the reduced χ^2 ratio which is around 1.0–1.2.

Calculation of Wobbling-in-Cone Angle. In our experiment the fluorescent probe (n-AS) is covalently attached to stearic acid and embedded in the lipid bilayer. The extent of probe wobbling within the membrane depends on the fluidity (order) of the membrane. The wobbling motion can be modeled as wobbling within a cone, whose semi angle (θ) can be calculated using the Kinosita model.¹² The semi angle of wobbling is given by:

$$\theta = \cos^{-1} \left[\frac{1}{2} \left\{ (1 + 8(r_\infty / r_0)^2)^{\frac{1}{2}} - 1 \right\} \right] \quad (10)$$

where $\theta = 90^\circ$ indicates free rotation. r_0 represents the anisotropy at zero time (initial anisotropy) in the anisotropy decay experiment and $r_\infty = r_0 \times \beta_s$, where β_s is the pre-exponential factor corresponding to the higher correlation time (slowly decaying component). Higher θ corresponds to the unrestricted rotation of the probe, while lower θ corresponds to the crowded or hindered rotation of the probe. The initial anisotropy (r_0) was estimated in a separate experiment in 70% glycerol in which all the motional dynamics slow down considerably. This value was kept fixed while analyzing the fluorescence anisotropy decay kinetics using eq (9).

Table S1**Time-Resolved Fluorescence Anisotropy Decay Parameters of n-AS probes
in DHPC and PLFE membranes^a**

Membrane	Probe	φ_1 (ns)	β_1	φ_2 (ns)	β_2	r_0
DHPC	2-AS	1.89 ± 0.08	0.48 ± 0.01	0.30 ± 0.02	0.52 ± 0.01	0.30
	6-AS	1.63 ± 0.09	0.48 ± 0.01	0.24 ± 0.03	0.52 ± 0.01	0.30
	9-AS	1.57 ± 0.02	0.44 ± 0.01	0.20 ± 0.01	0.56 ± 0.01	0.30
	12-AS	1.50 ± 0.02	0.29 ± 0.01	0.20 ± 0.01	0.71 ± 0.01	0.30
PLFE	2-AS	18.56 ± 0.80	0.52 ± 0.02	0.33 ± 0.05	0.48 ± 0.01	0.30
	6-AS	17.89 ± 0.70	0.55 ± 0.03	0.38 ± 0.01	0.45 ± 0.02	0.30
	9-AS	12.34 ± 0.04	0.58 ± 0.01	0.34 ± 0.01	0.42 ± 0.02	0.30
	12-AS	12.17 ± 0.03	0.62 ± 0.01	0.55 ± 0.02	0.38 ± 0.01	0.30

^an-AS was excited at 366 nm, and emission was collected at 460 nm using a combination of a monochromator and a 400 nm cutoff filter and measured with the TCSPC setup. See Experimental Section for other details. r_0 is the fundamental anisotropy of AS. The value of r_0 was kept constant at 0.3 in the analysis.

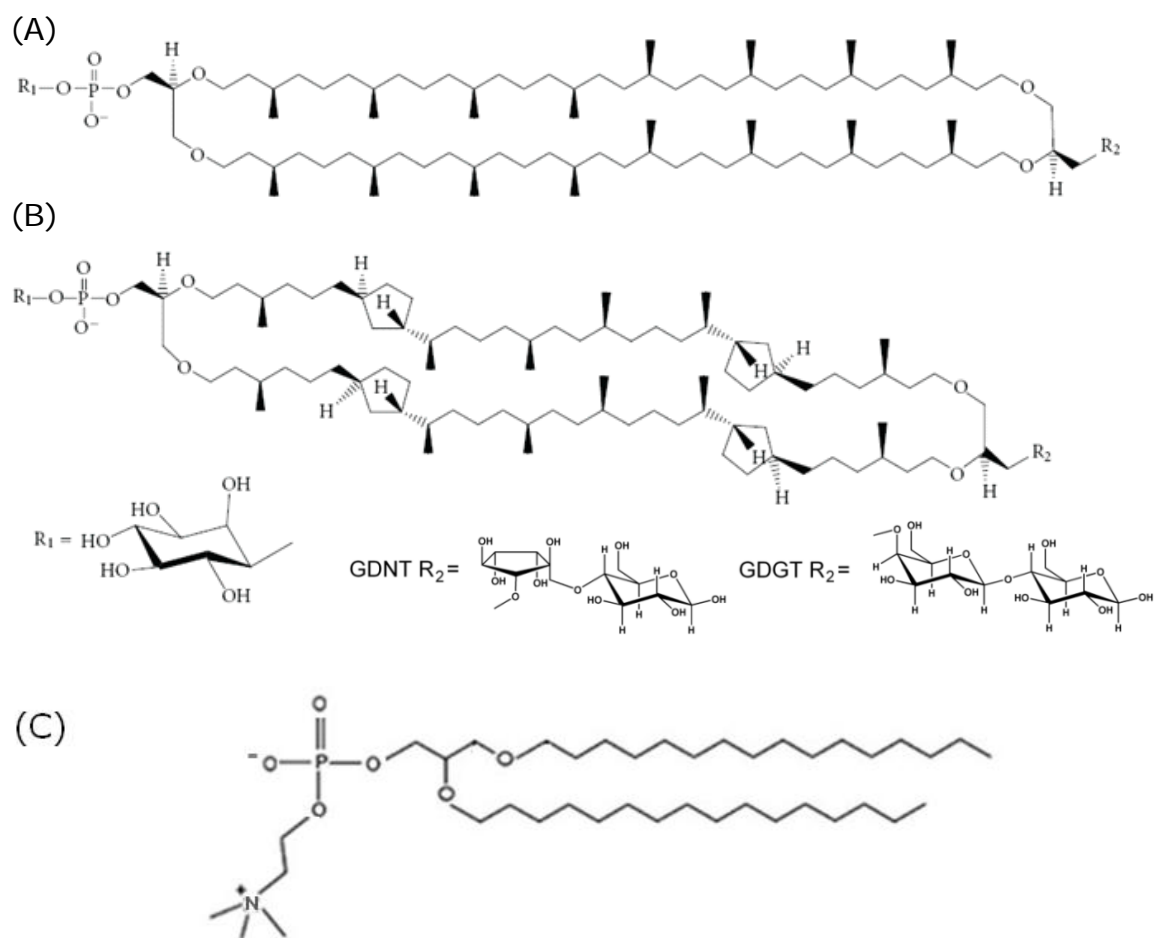


Figure S1. Chemical structures of the lipid components of bipolar tetraether lipid fraction E (PLFE) isolated from *S. acidocaldarius*. PLFE contains a mixture of tetraether lipids with either (A) glycerol dialkylglycerol tetraether (GDGT), or (B) glycerol dialkylnonitol tetraether (GDNT) skeleton. The number of cyclopentane rings in each biphytanyl chain can vary from 0 to 4. The different headgroups in GDGT and GDNT are presented at the bottom. (C) The chemical structure of DHPC.

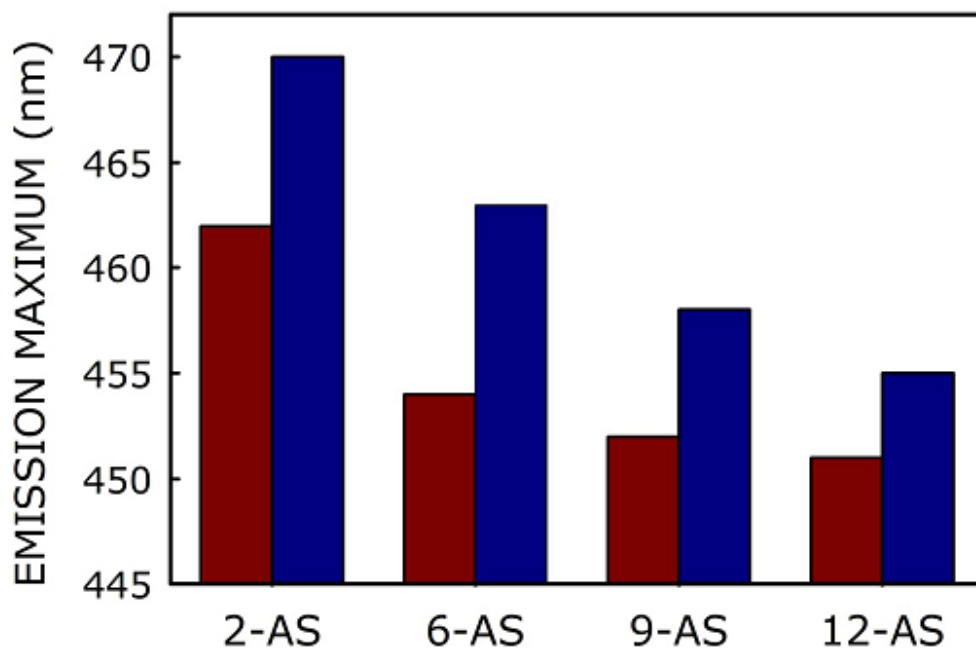


Figure S2. The emission maximum of n-AS probes in DHPC and PLFE membranes. Fluorescence emission maximum of n-AS probes in PLFE (maroon) and DHPC (blue) membranes for 2-AS, 6-AS, 9-AS and 12-AS. The ratio of probe to lipid was 1/100 (mol/mol) for DHPC and 1/50 (mol/mol) for PLFE, and the concentration of DHPC was 0.43 mM and that of PLFE was 0.21 mM. Experiments were carried out at $\sim 67^{\circ}\text{C}$ for both PLFE and DHPC membranes at pH 5. The excitation wavelength was 360 nm in both cases. See Experimental Section for other details.

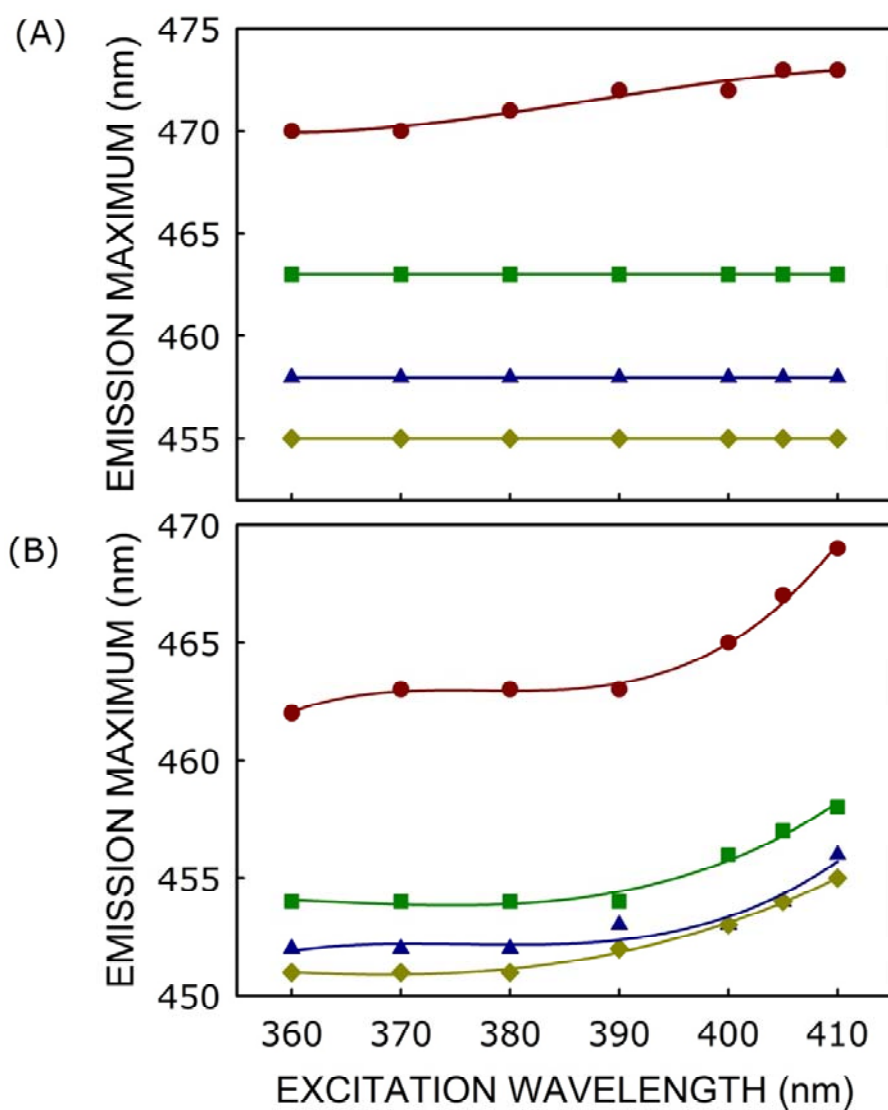


Figure S3. Effect of changing excitation wavelength on the wavelength of maximum emission of 2-AS (maroon, ●), 6-AS (green, ■), 9-AS (blue, ▲) and 12-AS (olive, ◆) in (A) DHPC, and (B) PLFE membranes. The lines joining the data points are provided merely as viewing guides. All other conditions are as in Figure 1. See Experimental Section for other details.

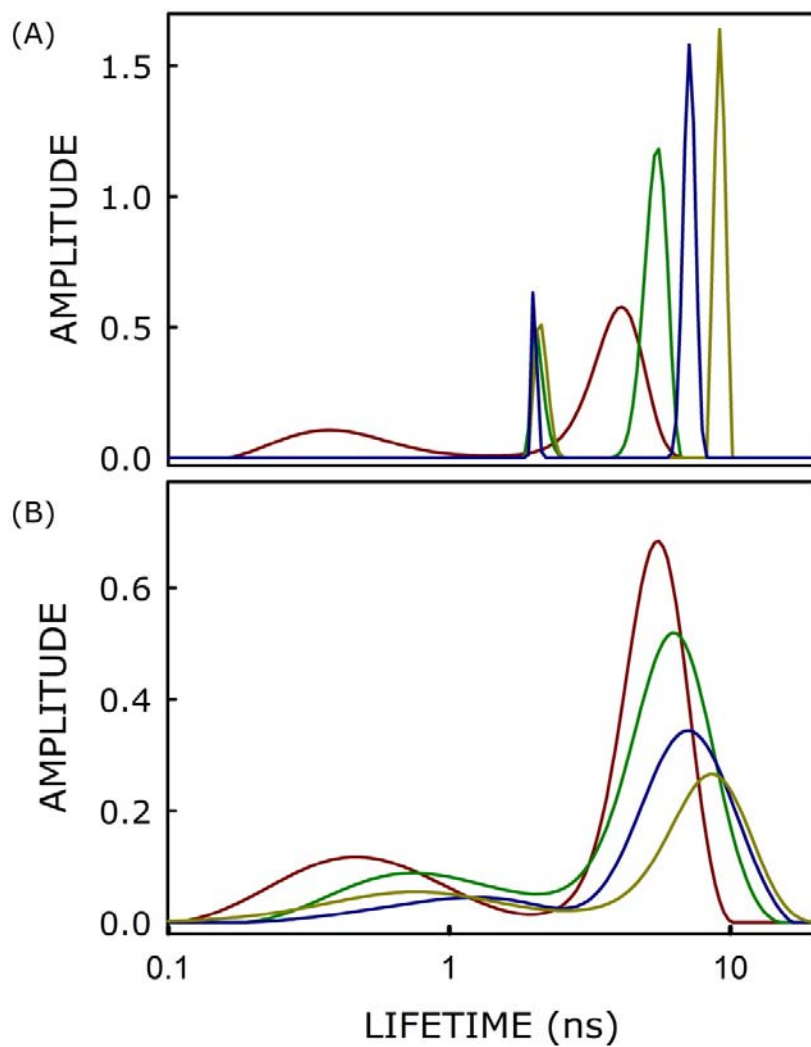


Figure S4. MEM lifetime distribution of n-AS probes in (A) DHPC and (B) PLFE membranes for 2-AS (maroon), 6-AS (green), 9-AS (blue) and 12-AS (olive). All other experimental conditions are same as in Figure 1. See Experimental Section for other details.

REFERENCES

1. Haldar, S.; Kombrabail, M.; Krishnamoorthy, G.; Chattopadhyay, A. Depth-dependent Heterogeneity in Membranes by Fluorescence Lifetime Distribution Analysis. *J. Phys. Chem. Lett.* **2012**, *3*, 2676-2681.
2. MacDonald, R. C.; MacDonald, R. I.; Menco, B. P. M.; Takeshita, K.; Subbarao, N. K.; Hu, L.-R. Small-volume Extrusion Apparatus for Preparation of Large, Unilamellar Vesicles. *Biochim. Biophys. Acta* **1991**, *1061*, 297-303.
3. Lakowicz, J. R. *Principles of Fluorescence Spectroscopy*; 3rd ed.; Springer: New York, 2006.
4. O'Connor, D. V.; Phillips, D. *Time-correlated Single Photon Counting*; Academic Press, London, 1984.
5. Bevington, P. R. *Data Reduction and Error Analysis for the Physical Sciences*; McGraw-Hill, New York, 1969.
6. Mukherjee, S.; Kombrabail, M.; Krishnamoorthy, G.; Chattopadhyay, A. Dynamics and Heterogeneity of Bovine Hippocampal Membranes: Role of Cholesterol and Proteins. *Biochim. Biophys. Acta* **2007**, *1768*, 2130-2144.
7. Haldar, S.; Kombrabail, M.; Krishnamoorthy, G.; Chattopadhyay, A. Monitoring Membrane Protein Conformational Heterogeneity by Fluorescence Lifetime Distribution Analysis using the Maximum Entropy Method. *J. Fluoresc.* **2010**, *20*, 407-413.
8. Brochon, J.-C. Maximum Entropy Method of Data Analysis in Time-resolved Spectroscopy. *Methods Enzymol.* **1994**, *240*, 262-311.
9. Swaminathan, R.; Krishnamoorthy, G.; Periasamy, N. Similarity of Fluorescence Lifetime Distributions for Single Tryptophan Proteins in the Random Coil State. *Biophys. J.* **1994**, *67*, 2013-2023.

10. Paila, Y. D.; Kombrabail, M.; Krishnamoorthy, G.; Chattopadhyay, A. Oligomerization of the Serotonin_{1A} Receptor in Live Cells: A Time-resolved Fluorescence Anisotropy Approach. *J. Phys. Chem. B* **2011**, *115*, 11439-11447.
11. Haldar, S.; Chaudhuri, A.; Gu, H.; Koeppel II, R. E.; Kombrabail, M.; Krishnamoorthy, G.; Chattopadhyay, A. Membrane Organization and Dynamics of "Inner Pair" and "Outer Pair" Tryptophan Residues in Gramicidin Channels. *J. Phys. Chem. B* **2012**, *116*, 11056-11064.
12. Kinoshita Jr., K.; Kawato, S.; Ikegami, A. A Theory of Fluorescence Polarization Decay in Membranes. *Biophys. J.* **1977**, *20*, 289-305.